Chronocoulometric determination of nitrate on silver electrode and sodium hydroxide electrolyte

Dohyun Kim, Ira Barry Goldberg and Jack William Judy*

Received 24th October 2006, Accepted 22nd January 2007
First published as an Advance Article on the web 15th February 2007
DOI: 10.1039/b614854a

An electrochemical system that consists of a silver electrode in 0.01 M sodium hydroxide electrolyte was investigated in an effort to develop a sensitive *in situ* analytical method for nitrate. Cyclic voltammetry demonstrated that the proposed system has a high normalized sensitivity (2.47 A $s^{1/2}$ $V^{-1/2}$ M^{-1} cm^{-2}), compared to more complex electroanalytical schemes. Double-potential-step chronocoulometry was used to maximize the signal-to-noise ratio (SNR), and minimize interference from dissolved oxygen in the electrolyte. The integration period for double-potential-step chronocoulometry was determined by optimizing the extended Cottrell equation. The integrated current is proportional to nitrate up to 10 mM and the average detection limit is approximately 1.7 μM. Dissolved oxygen does not degrade performance. To examine the potential interference of other ions when analyzing nitrate, we measured the electrode response to 1000 μM each of NO_2^-, Cl^-, PO_4^{3-}, SO_4^{2-}, F^-, CO_3^{2-}, BO_2^-, K^+, Ca^{2+}, and Sr^{2+} with and without 1000 μM nitrate. Interference is negligible for most of the ions when nitrate is absent (*i.e.* <1% of the response to equimolar nitrate). However, interference is substantial (>20% increase or decrease in the electrode response to nitrate) for PO_4^{3-}, Ca^{2+}, and Sr^{2+} when equimolar nitrate is present.

Introduction

This study was undertaken to develop and validate an electroanalytical method of measuring nitrate concentration for use in a sensor that could, eventually, be mass-produced, stand-alone, and field-deployable.

Nitrate is an anion of major importance because it is virtually everywhere (*e.g.* food, soil, groundwater, sea water, and surface water), and can contaminate water supplies because of high solubility in water. The most pervasive source of contamination is fertilizer runoffs to streams and diary farm feces that leach into groundwater.[1] Nitrate ingestion above a critical level causes significant clinical problems. Specifically, nitrate is considered to be the cause of *methemoglobinemia* in infants and may be a cause of bladder cancer, gastric cancer, and leukocyte enzyme abnormality.[2,3]

Effective monitoring would require large-scale deployment and interrogation of a network of real-time nitrate sensors. Distributed nitrate sensors could enable more intelligent applications (*e.g.* contaminant-zone assessment, contaminant-transport-parameter estimation, and reclaimed-water irrigation management[4,5]). A common requirement to all of these applications is for the sensor to be used frequently over a long period of time and over a large area without frequent human intervention. Also, a small form-factor is desirable so that it does not interfere with the environment. Consequently, the nitrate sensors will need to be sensitive, small, low-power, and reliable for long-term field deployment.

Electrical Engineering Department, University of California, Los Angeles, Los Angeles, CA 90095, USA. E-mail: jack.judy@ucla.edu; Fax: +1-310-861-5055; Tel: +1-310-206-1371

Traditional bench-top nitrate-analysis techniques, based on UV/Vis spectrometry,[6] gas chromatography,[7] ion chromatography,[8] HPLC,[9] or capillary electrophoresis,[10] usually require expensive and massive instrumentation, complex measurement procedures, and thus are not suitable for a sensor that satisfies requirements of the aforementioned applications. Electrochemical methods, such as amperometry and potentiometry, are sufficiently sensitive for the targeted measurement range,[11] are relatively simple to operate, easy to miniaturize, and less power-hungry. Therefore, an electrochemical sensor should be amenable to the long-term deployment. Of these electrochemical methods, amperometry generally offers higher precision, lower detection limits,[11] and easier miniaturization because an internal reference solution is not needed. Among amperometric techniques, chronocoulometry has distinct advantages[12] over amperometry: chronoamperometric signals decay with time but chronocoulometric signals increase with time; integration is effective in improving the signal-to-noise ratio (SNR); separating the non-faradaic double-layer charge from the faradaic charge is easier. Double-potential-step chronocoulometry is the electroanalytical technique used in this study because the analytical performance is better, and oxygen reduction can be easily separated from the nitrate reduction due to its more positive reduction potential. Also, to the best of our knowledge, chronocoulometry has not been used for nitrate analysis as a means of improving the SNR and minimizing oxygen interference.

Amperometric nitrate sensors can exist as commercial electrodes in macroscopic flow-injection analysis systems[13,14] or as microfabricated electrodes in highly miniaturized analysis systems.[15,16] A solid metal working electrode was investigated rather than a non-metal electrode (*e.g.* carbon or

mercury drop) or a surface-modified electrode (*e.g.* freshly deposited metal complexes,[17] catalytic metals,[18] or immobilized biological catalysts[19]) because the solid metal electrode can be easily adapted to both macroscale and microscale sensors and the surface can be regenerated if it is contaminated. Direct amperometric nitrate determinations on various metal electrodes in aqueous media have been reported.[20–27] Despite thermodynamic feasibility,[28] many metal electrodes failed to demonstrate high sensitivity to nitrate reduction due to slow kinetic processes throughout the pH range.[26] Transition metals, especially those in the groups Ib and IIb show the highest activity for nitrate reduction in mild acidic and basic electrolytes.[26] Studies of nitrate reduction on silver and silver-composite electrodes with appropriate surface activation show that silver has the highest sensitivity for reducing nitrate to nitrite, or further to ammonia.[25–27] Reduction peaks are well separated from hydrogen evolution in alkaline media. Therefore, we studied cathodic nitrate reduction on silver disk electrodes in NaOH electrolyte and confirmed its feasibility as a sensitive nitrate detection method.

Common ions can interfere with the proposed nitrate analysis. Since we are interested in water-quality monitoring as a future application of the analytical method, we quantified the interference for ten of the common ions present in groundwater (NO_2^-, Cl^-, PO_4^{3-}, SO_4^{2-}, F^-, CO_3^{2-}, BO_2^-, K^+, Ca^{2+}, and Sr^{2+})[29] in two ways: first, we measured the signal due to the presence of the interfering ions and converted the chronocoulometric signal to an equivalent nitrate concentration derived from nitrate standards; second, we examined the effect of the interfering ions on the signal in the presence of a known nitrate concentration.

Experimental

Chemical reagents

16 MΩ cm deionized (DI) water from a Super-Q™ Plus High Purity Water System (Millipore, Billerica, MA, USA) was used. All chemicals are ACS reagent grade. Sodium hydroxide solutions were freshly prepared from pellets (EM Science, Gibbstown, NJ, USA) before each experiment. A 0.1 M nitrate standard (Thermo Orion, Waltham, MA, USA) was sequentially diluted for nitrate measurements. For the interference study, 1 M ion standards were prepared with sodium or acetate salts: NaCl, Na_3PO_4, and $NaC_2H_3CO_2{\cdot}3H_2O$ were made from Fisher Scientific Co. (Hampton, NH, USA), $NaNO_2$, and NaF from Aldrich Chemical Co. (Milwaukie, WI, USA), $NaBO_2{\cdot}4H_2O$ and $Sr(C_2H_3O_2)_2{\cdot}xH_2O$ from Sigma-Aldrich (St. Louis, MO, USA), Na_2SO_4 and Na_2CO_3 from EMD Chemical Inc. (Gibbstown, NJ, USA), and $KC_2H_3O_2$ and $Ca(C_2H_3O_2)_2{\cdot}H_2O$ in Mallinckrodt and Baker (Phillipsburg, NJ, USA). The sodium hydroxide solutions were purged with a purified argon gas (Air Liquide America L.P., Santa Fe Springs, CA, USA) for more than 10 min before each experiment.

Electrode preparation

Two silver electrodes were used in this study. A 0.5 mm-diameter electrode was made with 99.99% silver wire (Alfa Aesar, Ward Hill, MA, USA) encased in a 10 ml plastic syringe body with Epoxy for fundamental electrochemical studies. A 1.6 mm-diameter polycrystalline silver disk electrode (Bioanalytical System Inc., West Lafayette, IN, USA) was used for double-potential-step chronocoulometry of nitrate. Before experiments, they were mechanically polished with 800 grit and 1000 grit polishing pads and then with an 0.3 μm-diameter alumina-particle suspension on Microcloth™ pads. All the polishing supplies were obtained from Buehler (Lake Bluff, IL, USA). Polished silver electrodes were rinsed with DI water in an ultrasonic bath. Electrochemical activation was performed by sweeping the potential from −1.2 to 1.0 V *vs.* Ag/AgCl reference electrode (unless otherwise stated) at a sweep rate of 1 V s^{-1} 20 times, followed by 20 potential pulses between −0.25 and 0.9 V (0.5 s pulse width).

Apparatus

A PC-connected potentiostat (PAR-283, Princeton Applied Research, Oak Ridge, TN, USA) was used for basic electrochemical studies and the cyclic voltammetry of nitrate on the silver disk electrodes. Chronocoulometric measurement was conducted with an electrochemical workstation (CHI-660B, CH instrument, Austin, TX, USA). All measurements were performed in a Faraday Cage (CHI- 200, CH instrument, Austin, TX, USA). Either Fischer Scientific Accumet Ag/AgCl or Bioanalytical System Inc. RE-5B Ag/AgCl reference electrodes were used.

Result and discussion

Cyclic voltammetry

Nitrate reduction in alkaline media[27] can occur as a two- or eight-electron process according to eqn (1):

$$NO_3^- + H_2O + 2e^- \rightarrow NO_2^- + 2OH^- \quad (1a)$$

$$NO_3^- + 6H_2O + 8e^- \rightarrow NH_3 + 9OH^- \quad (1b)$$

Several groups reported that silver has excellent activity for reducing nitrate.[25–27] Cattarin[25] reported that nitrate reduces to 90–94% nitrite and 1–3% ammonia during constant-potential electrolysis at −1.4 V (*vs.* SCE) in 1 M NaOH. Electrochemical reduction of nitrate in alkaline electrolyte is of interest because hydroxide shifts the reduction of water ($2H_2O + 2e^- \rightarrow H_2 + 2OH^-$) negative with respect to nitrate reduction. This allows a well-defined nitrate-reduction wave. Fig. 1 shows a cyclic voltammogram of nitrate with a silver disk electrode in 1 M NaOH electrolyte. The nitrate-reduction wave [Fig. 1(b)] shows a cathodic peak with no reversible anodic peak. Nitrite, a product of the electrochemical reaction given in eqn (1a), may reduce to NH_3 at a potential more negative than −1.2 V, but any distinct reduction peak would be obscured by the large hydrogen evolution current. Both curves of Fig. 1 show an anodic peak at −0.65 V, which Savinova *et al.*[30,31] propose is caused by hydroxide electrochemisorption. A cathodic hydroxide desorption peak[30,31] is seen at −1.0 V in Fig. 1(a) but not in Fig. 1(b), due to a large nitrate-reduction current. The peak current decreases

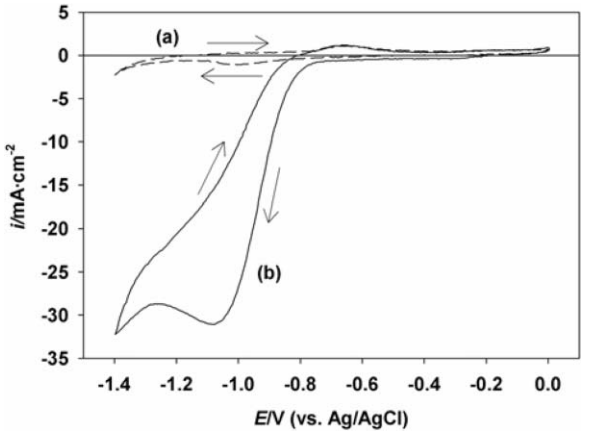

Fig. 1 Cyclic voltammograms (0.05 V s^{-1}) performed with a stationary silver electrode in 1 M NaOH electrolyte. Curve (a), which is obtained with a blank electrolyte, illustrates the background current. Curve (b) is obtained with 100 mM nitrate and the nitrate-reduction peak is clearly shown.

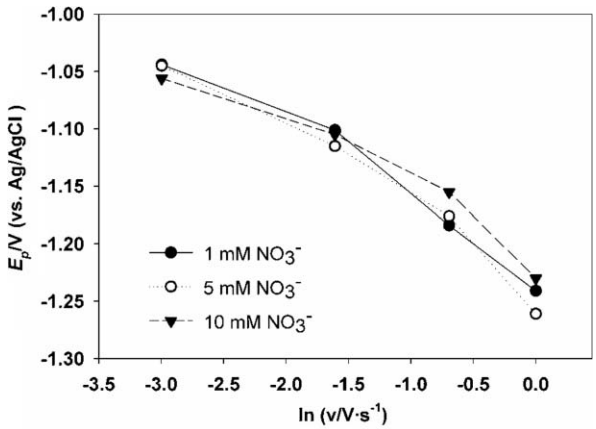

Fig. 2 Cathodic peak voltage for nitrate reduction in a 1 M NaOH electrolyte at various voltage sweep rates.

appreciably with repetitive voltage sweeps, indicating nitrate depletion. The absence of a reverse oxidation wave shown in Fig. 1 and the negative shift of peak potential with increasing scan speed (0.05 to 1 V s^{-1}), shown in Fig. 2, demonstrate that reaction (1a) is an irreversible process. Nevertheless, we speculate that the current is controlled by diffusion from the fact that the peak current i_p is proportional to the square root

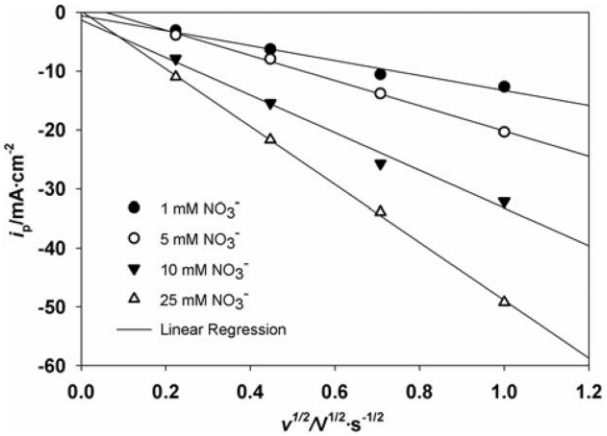

Fig. 3 Cathodic peak current of nitrate in 1 M NaOH electrolyte at various voltage sweep rates.

of the scan speed v (Fig. 3). We find that peak current, i_p, is proportional to nitrate concentration up to 50 mM.

To verify if silver electrodes exhibit the highest sensitivity, a normalized sensitivity, $\bar{i}_p$, is defined as

$$\bar{i}_p = \frac{i_p}{nAv^{1/2}C_o^*} \quad \left(\frac{\text{A s}^{1/2}}{\text{V}^{1/2}\ \text{M cm}^2}\right) \tag{2}$$

where n is the number of electrons in the reduction step, A is the surface area of electrode (cm^2), v is the potential sweep rate (V s^{-1}), and C_o^* is the bulk concentration of nitrate (M). Table 1 shows the normalized sensitivity, $\bar{i}_p$, calculated for nitrate reduction in different electrochemical systems with the experimental parameters obtained from literature. We let $n = 2$ [eqn (1a)] for all cases, unless literature notes otherwise. Our silver working electrode shows greater sensitivity than other work, except Cox and co-workers[35] in which a complexing agent was included in the electrolyte.

Minimizing interference from oxygen reduction with double-potential-step measurement

About 0.3 mM of oxygen is present in air-saturated aqueous solution[36] and oxygen reduces in alkaline media according to

$$O_2 + 2H_2O + 4e^- \rightarrow 4OH^-. \tag{3}$$

Since oxygen reduction occurs at a more positive potential than nitrate reduction, the large current from the oxygen reduction interferes with the nitrate measurement. A

Table 1 Normalized peak current for amperometric detection of nitrate

$\bar{i}_p$ $\left(\frac{\text{A s}^{1/2}}{\text{V}^{1/2}\ \text{M cm}^2}\right)$	v/V s^{-1}	A/cm^2	Electrolyte	Electrode	Reference
2.47	0.01	0.00196	0.01 M NaOH	Silver	This work
1.3	0.002	1.2	0.5 M H_2SO_4 + 0.1 mM KCl + 0.01 M $CuSO_4 \cdot 5H_2O$	Copper-plated carbon	Edmonds and co-workers[32]
0.43	0.01	18.0	0.1 M Na_2SO_4 + 0.1 M HCl	Copper-plated copper	Compton and co-workers[33]
0.77	0.1	0.196	0.1 M NaH_2PO_4 + 10 μM $CdCl_2$ + 50 μM $CuCl_2$	Copper/cadmium-plated pyrolytic graphite	Bodini and Sawyer[34]
0.85	0.1	0.196	0.1 M KCl + 0.2 mM $CdCl_2$ + 0.01 M HCl + 1.0 mM $CuCl_2$	Copper/cadmium-plated pyrolytic graphite	Bodini and Sawyer[34]
14	0.010	0.034	0.1 M KCl + 0.01 M $LaCl_3$	Hanging mercury drop	Lundquist and co-workers[35]

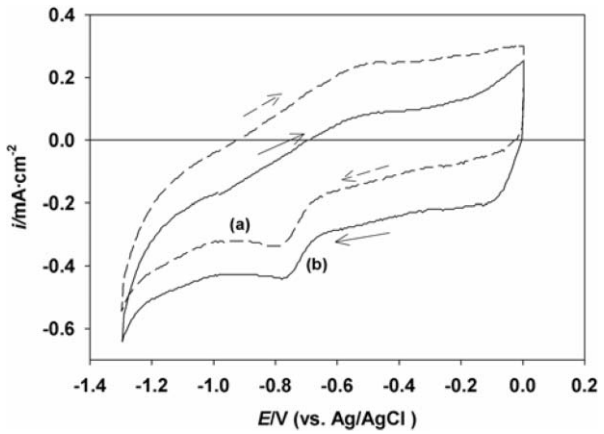

Fig. 4 Cyclic voltammograms (50 mV s^{-1}) for the reduction of 0.1 mM nitrate in a 0.01 M NaOH electrolyte (a) with oxygen purged by argon and (b) without purging.

substantial increase (−0.16 mA cm^{-2}) in baseline current is observed as shown in Fig. 4 when the 0.01 M NaOH electrolyte was not purged with argon [curve (b)] as compared to a purged solution [curve (a)].

Interference from dissolved oxygen can be removed by purging with an inert gas, electrolysis,[37] photochemical processing,[38] and permeation through a semi-permeable membrane.[39] However, these methods are unsuitable for field-deployable sensors because they require complex additional fabrication and/or toxic chemicals. Instead, the difference between the nitrate- and oxygen-reduction peak potentials is exploited with a potential-pulse sequence. First, the potential is held at $E_1 = -0.5$ V where the reduction of dissolved oxygen proceeds in a diffusion-limited regime. This potential is maintained for more than 2 s, which is sufficient for the cathodic current to reach a steady-state. Next, the potential is stepped to $E_2 = -0.93$ V, where nitrate reduction is diffusion-limited but more positive than the start of hydrogen evolution. Although oxygen reduction is ongoing in a diffusion-limited fashion at this potential, its current is small and nearly constant. To determine the nitrate concentration, the current should be measured a short time after the potential is biased at E_2 but before steady-state diffusion occurs and nitrate-reduction current becomes small. Fig. 5(a) shows a typical current response with respect to time when the potential of the working electrode is stepped first to E_1 then to E_2 [Fig. 5(b)]. The transient current in response to E_1 is independent of nitrate concentration and reaches a steady-state in about 2 s. The nitrate-reduction current can be obtained by subtracting the steady-state oxygen-reduction current at E_1 from the non-steady-state nitrate-reduction current at E_2.

Double-potential-step chronocoulomety of nitrate

Instead of measuring the current to determine the nitrate concentration, the current is integrated numerically over a time period to yield charge (chronocoulometry) as a measurement of nitrate concentration. The measured current contains non-faradaic current due to double-layer charging and noise, and

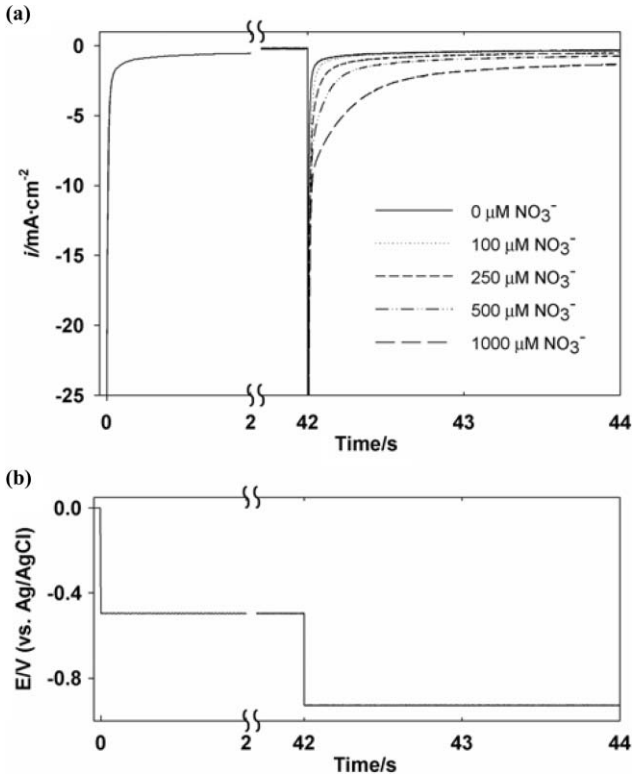

Fig. 5 (a) Current response and (b) a potential-step sequence for nitrate reduction of various concentrations in a 0.01 M NaOH electrolyte.

faradaic residual currents. In order to maximize the SNR of the analytical method, subject to the unwanted signal, the integration duration needs to be optimized. Therefore, an objective function, based on a mathematical model of the electrochemical processes, needs to be obtained. If nitrate reduction were controlled by semi-infinite linear diffusion, the time dependence of the faradaic-reduction current, I_d, would follow the Cottrell equation. The linear diffusion approximation would be sufficiently precise when the parameter τ, indicating the extent of the non-linear diffusion,

$$\tau = 4D_o t/R^2 \quad (4)$$

is small.[40] For given dimension of disk electrode, R, and time scale of chronocoulometry, t, the parameter τ is about 0.24, where $D_o = 1.910 \times 10^{-5}$ cm^2 s^{-1} (diffusion coefficient of nitrate in infinite dilution[41]), $t = 20$ s, and $R = 0.08$ cm. Rigorous expressions for diffusion-controlled currents at a stationary finite disk electrode[42] predict that there is significant deviation from the Cottrell equation (*i.e.* 45% deviation for $\tau = 0.24$). The deviation will be even greater in chronocoulometry because the current is integrated over a long period. Appreciable stationary current is always observed experimentally within the time scale even after the double-layer charging current and residual current are removed numerically from the amperometric response. Lingane observed such phenomena in chronoamporomety with a platinum disk electrode of 0.258 cm radius.[43] To account for the deviation, the Cottrell equation is modified by expanding it in a power series of $(D_o t/R^2)^{1/2}$.

Higher order terms are discarded in the series because the first-order term is significant[44,45] as long as the assumption of semi-infinite diffusion remains valid. The modified diffusion-limited current response on a finite disk electrode is given by

$$I_d = \frac{nFAD_o^{1/2}C_o^*}{\pi^{1/2}t^{1/2}}\left\{1 + B\sqrt{\frac{D_o t}{R^2}}\right\} \quad (5)$$

where F is the Faraday constant, t is time, and B is an empirical coefficient for the second term in the series. Because of the double-layer charging in an electrode–electrolyte interface, an exponentially decaying component I_c is also added to the measured current,

$$I_c = (\Delta E/R_s)\exp^{-(t/R_s C_d)} \quad (6)$$

where ΔE is the applied potential step, R_s is the uncompensated resistance of the cell, and C_d is the double-layer capacitance. In reality, C_d is a function of the applied voltage and thus a function of time, rather than being constant. The simple exponential decay predicted by eqn (6) may not be the actual representation of the double-layer charging.

A small residual current, I_r, contributes to the total current. This can be due to the reduction of trace-quantities of electroactive species, a small amount of hydrogen reduction, reduction of adsorbed species, or reduction of silver oxides formed on the electrode surface. So the total measured current, I_{total}, is given by

$$I_{total} = I_d + I_c + I_r. \quad (7)$$

It should be noted that I_r is significant even for thoroughly purged blank electrolyte. Curve (a) in Fig. 6 shows a 20.3 μA cm^{-2} residual current in the blank electrolyte, even 20 s after a potential step. Curve (b) shows the steady-state current due to radial diffusion of 500 μM nitrate as predicted by eqn (5). The double-layer-charging current decays to a negligible value after about 0.5 s (*i.e.* <1% of the initial current measured at t = 0 after the potential step to E_2).

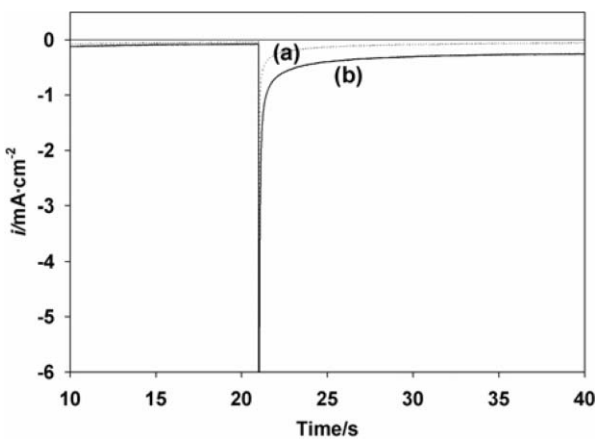

Fig. 6 Chronoamperometric response to a potential step for (a) 0.01 M NaOH blank electrolyte, and (b) the reduction of 500 μM nitrate in the same electrolyte.

For chronocoulometric measurements, faradaic charges, Q_d, can be expressed as

$$Q_d = \left|\int_0^t I_d dt\right| = \frac{2nFAD_o^{1/2}C_o^* t^{1/2}}{\pi^{1/2}} + \frac{nBFAD_o C_o^*}{\pi^{1/2}R}t. \quad (8)$$

The faradaic charge is proportional to the bulk concentration of the electroactive species C_o*. The bigger Q_d for the same C_o* is preferred for sensitive nitrate detection. The non-faradaic current integrated for a time period t is given by

$$Q_c = EC_d\left[1 - \exp^{-\left(\frac{t}{R_s C_d}\right)}\right] + I_r t. \quad (9)$$

and has a role as a measurement background. For sensitive measurements, the SNR must be maximized for the integration time t. SNR can be defined as $S(t) = Q_d/(Q_n C_o^*)$ where Q_n is a noise component of the integrated currents. Weber and co-workers[46,47] characterized sources of noise in typical amperometric detectors (*e.g.* input voltage/current noise in the current-to-voltage converter, impedance noise, Johnson noise in faradaic process/solution resistance, and shot noise). We neglect Johnson noise, shot noise, and input current noises because of their small magnitude (*ca.* 0.1–10 pA Hz$^{-1/2}$) compared with the 129.1 pA Hz$^{-1/2}$ ADC (analog-to-digital converter) quantization noise of the CHI 660B potentiostat (*i.e.* a 12 bit ADC and 10 nA resolution setting). Weber also observed that the major sources were impedance noise and input voltage noise. We assume, for the sake of simplicity, that white noise including quantization noise is dominant. Therefore, an average power of the integrated current white noise $Q_n(t)$ is given by

$$Q_n = \left(\int_0^t I_n(t)dt\right)^{1/2} = \beta t^{1/2} \quad (10)$$

where β is a proportionality constant related to noise power. For maximum SNR, the object function $S(t) = Q_d/(Q_n C_o^*)$ needs to be optimized with respect to t. $S(t)$ can be expressed as

$$S(t) = \frac{2nFAD_o^{1/2}}{\pi^{1/2}\beta} + \frac{nBFAD_o t^{1/2}}{\pi^{1/2}\beta R} \quad (11)$$

where the stoichiometric number n = 2 for the two-electron reduction of nitrate [eqn (1a)], the Faraday constant F = 96485.3 C, the radius of the disk electrode R = 0.025 cm, and the geometric surface area A = 1.963 × 10^{-3} cm^2. Similar to Lingane's work,[43] the proportionality constant B and the diffusion coefficient D_o of eqn (11) are obtained from the chronoamperometric response of nitrate, $I_d t^{1/2}/(AC_o^*)$ *vs.* $t^{1/2}$, which is given by

$$\frac{I_d t^{1/2}}{AC_o^*} = \frac{nFD_o^{1/2}}{\pi^{1/2}}\left\{1 + B\sqrt{\frac{D_o t}{R^2}}\right\}. \quad (12)$$

After plotting eqn (12), a linear regression is performed with respect to $t^{1/2}$ as shown in Fig. 7. D_o is calculated from the

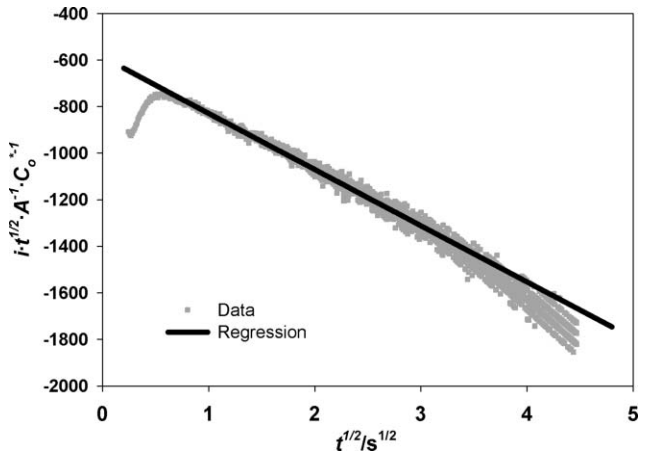

Fig. 7 Plot and linear regression used for determining the chronoamperometric constant (500 μM nitrate in a 0.01 M NaOH electrolyte).

y-intercept value and B is obtained from the slope. Four identical experiments were repeated and average values are $D_o = 2.71 \times 10^{-5}$ cm^2 s^{-1} and $B = 3.81$. The double-layer-charging current for a 0.01 M NaOH solution was subtracted from the responses of the 500 μM nitrate solution to determine the true faradaic current, I_d. Currents were sampled for 20 s after the step. The early transient response (*ca.* 0–0.36 s) and late transient (after *ca.* 9 s) were not used in the regression due to deviation from ideality. The reason for the deviation at short times is speculated to be a larger effective surface area due to the microscopic surface morphology of the roughened silver electrode, and the late transient was the result of convection.[43,48]

For an arbitrary constant for faradaic noise, $\beta = 1$, $S(t)$ increases monotonically with the square root of t. Therefore, as the integration time increases, the SNR increases. However, Fig. 7 shows that convection causes deviation from the extended Cottrell eqn (5) after approximately 9 s. This limits the integration time because convection could cause random errors in the analytical measurements. Also, the first 40 ms of the current transient was truncated because of the limited dynamic range of the potentiostat. The maximum detectable current is ±20.47 μA at 10 nA resolution.

Calibration curves for nitrate are shown in Fig. 8. The silver working electrode was electrochemically activated before each measurement. Data were obtained in two ways: for Fig. 8(a) the solution was not purged with inert gas. An initial potential of −0.5 V was applied for 20 s to reduce the oxygen-reduction current. A small amount of residual current for oxygen still exits, and the current is integrated for 1 s, starting 19 s (Q_1). Then the potential was stepped to −0.93 V for nitrate and oxygen reduction, and the current was integrated for 1 s, starting 40 ms after the potential step (Q_2). The nitrate-reduction charge was determined by subtracting the charge Q_1 from Q_2, because Q_1 contains oxygen-reduction charge and Q_2 equals the sum of the oxygen- and nitrate-reduction charges. The second method of obtaining the data was same as the first, except that the solution was purged with argon [Fig. 8(b)].

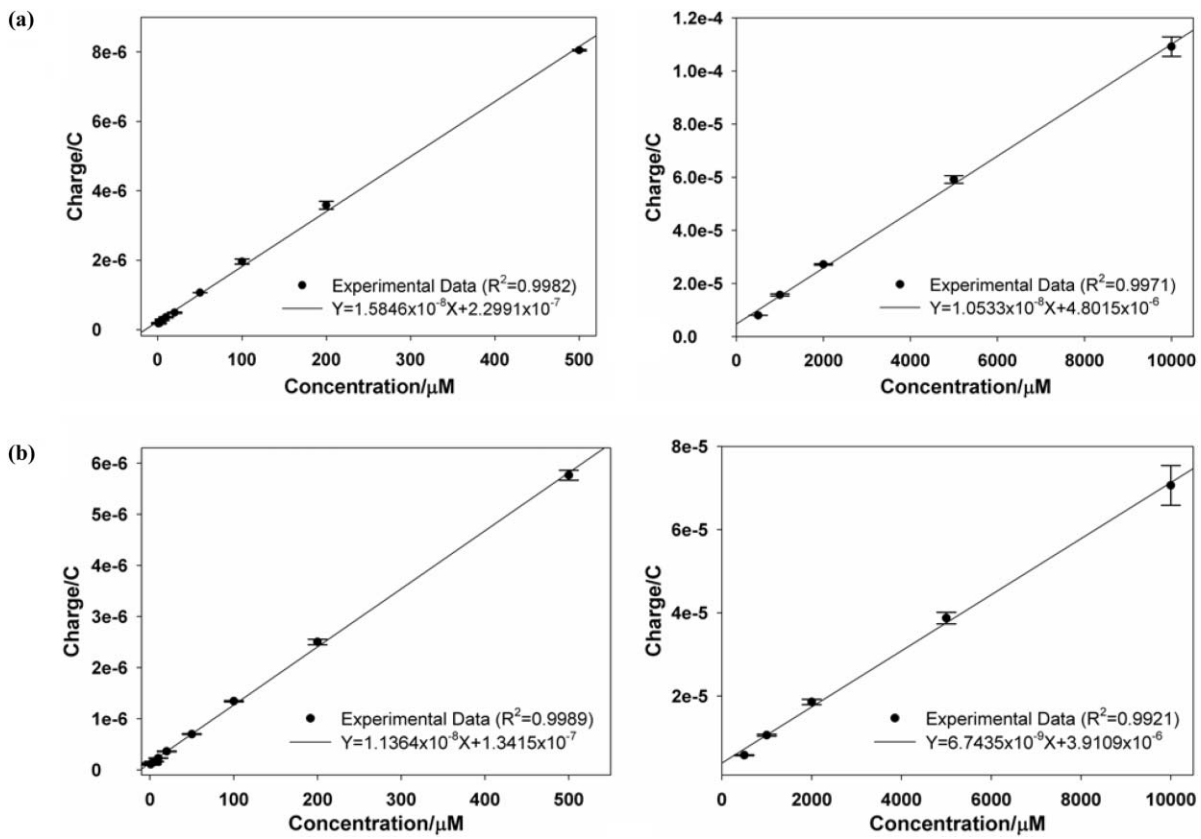

Fig. 8 Chronocoulometric calibration curves for nitrate in a 0.01 M NaOH electrolyte (a) not purged with argon, and (b) purged with argon.

Known nitrate concentrations of 1, 2, 5, 10, 20, 50, 100, 200, 500, 1000, 2000, 5000, 10 000 μM were prepared using the standard addition method. The integrated current was plotted with respect to concentration and the slope was calculated using linear regression. We find that calibration curves are linear in two ranges with different slopes: (1) from 1 to 500 μM, and (2) from 500 to 10 000 μM. The correlation coefficient R^2 is about 0.99 in almost all cases. For each case, experiments were duplicated and two calibration curves were obtained.

The detection limit in concentration, C_{dl}, was calculated as $C_{dl} = (\bar{X}_{dl} - \bar{X}_b)/s$ where s is a slope of a calibration curve, $\bar{X}_{dl}$ ($=\bar{X}_b + z\sigma_b$) is the detection limit in charge (C), $\bar{X}_b$ and σ_b are, respectively, the mean and standard deviation of the integrated current of the blank solution, and z is a predetermined confidence level.[49] We chose $z = 3$ as Kaiser[50] suggested. The average detection limit, C_{dl}, was 1.7 μM when the electrolyte was purged with argon. An important result is that the detection limits of unpurged solutions are similar to those of purged solutions (*i.e.* 2.6 μM compared with 1.7 μM). Also, the detection range is the same and the slope is not decreased. We conclude that double-potential-step chronocoulometry of nitrate successfully rejects oxygen interference from this result.

Interference study

Interference from ions in commonly present in groundwater was determined with the same electrochemical system and techniques. 1 M standards of each of seven anions [NO_2^-, Cl^-, PO_4^{3-}, SO_4^{2-}, F^-, B (as BO_2^-), and CO_3^{2-}], and three cations (K^+, Ca^{2+}, and Sr^{2+}) were prepared with reagent grade salts. Only K^+, Sr^{2+}, and Ca^{2+} were tested due to very low solubility of other metal hydroxides in alkaline media (*e.g.* Fe^{3+} and Mg^{2+}). The interference results are presented in Table 2. Two kinds of interference were studied: (1) how much the electrochemical system mistakenly could sense nitrate from the interfering ions when nitrate is absent, and (2) how much the nitrate measurement could be affected by the interfering ions when nitrate is present.

For the first study, a calibration curve was determined using nitrate standards before each measurement of interfering ions. Then, 1000 μM solutions of each of the interfering ions in fresh electrolyte were measured. An analytic signal was determined and related to an equivalent nitrate concentration using the nitrate calibration curves. The interference is, in general, minimal (*i.e.* less than 1% of response relative to 1000 μM nitrate). NO_2^- is a common problem in nitrate analysis but the interference is equivalent to 3.9 μM nitrate in this study. The largest interference arises from PO_4^{3-} (equivalent to 6.9 μM nitrate) but is still a small value. The signal from SO_4^{2-}, F^-, CO_3^{2-}, BO_2^-, K^+, and Sr^{2+} are smaller than the average nitrate detection limit C_{dl}.

For the second study, a calibration curve was obtained in the same way as the first study. A 1000 μM nitrate solution in the electrolyte was prepared and the analytic signal was measured. Then, a sufficient amount of 1 M standard of one of the interfering ions was pipetted to the nitrate solution to yield 1000 μM of the interfering ion. The analytic signal was again measured and the equivalent nitrate concentration was calculated using the nitrate calibration curve. The previously measured concentration of nitrate-only solution was compared with the equivalent concentration determined for the solution with interfering ions. In general, the equivalent nitrate concentration increases or decreases by less than 10%. PO_4^{3-} anions and Ca^{2+} and Sr^{2+} cations can be potential problems since these either increase or decrease the equivalent nitrate concentration by more than 20% when they are present in large quantity. Although F^- has on average a negligible effect on the nitrate analysis, it causes a large measurement variation. We do not know the reason for this result. Acetate salts were used for cation standards because the acetate ion (as 1 mM $NaC_2H_3O_2$) showed negligible interference by itself (Table 2). It is worthwhile to note that a 2.4% increase is observed with acetate ion for the second study, as the table footnote indicates. Therefore, this fact should be considered when interpreting the results for cation interferences.

Conclusions

This electrochemical analysis of nitrate demonstrates greater sensitivity than other more complex electrochemical methods previously investigated. Double-potential-step chronocoulometry has two benefits: (1) theoretical analysis shows an increase in the signal-to-noise ratio with a long integration time; (2) interference from oxygen in the electrolyte was subdued and the detection limit, concentration range and sensitivity do not deteriorate. The proposed technique demonstrates promising performance as a sensitive nitrate-analysis technique. The average detection limit of double-potential-step

Table 2 Equivalent nitrate concentration of 1000 μM ionic species

Ions	Added as 1000 μM of each	Equivalent NO_3^- concentration (0 μM NO_3^-)	Standard deviation	Equivalent NO_3^- concentration (1000 μM NO_3^-)	Standard deviation
PO_4^{3-}	Na_3PO_4	6.9	1.4	737	23
Cl^-	NaCl	4.1	3.3	920.92	0.70
NO_2^-	$NaNO_2$	3.9	1.1	923.5	9.6
CO_3^{2-}	Na_2CO_3	$<C_{dl}$	—	1059	25
SO_4^{2-}	$Na_2(SO_4)$	$<C_{dl}$	—	943	14
BO_2^-	$NaBO_2$	$<C_{dl}$	—	1030	38
F^-	NaF	$<C_{dl}$	—	1002	42
Ca^{2+}	$Ca(C_2H_3O_2)_2$	2.4	1.4	1264[a]	27[a]
Sr^{2+}	$Sr(C_2H_3O_2)_2$	$<C_{dl}$	—	1208[a]	16[a]
K^+	$K(C_2H_3O_2)$	$<C_{dl}$	—	1038.8[a]	2.6[a]

[a] Acetate ion (added as $NaC_2H_3O_2$) presents 1024 μM of interference.

chronocoulometry was about 1.7 μM and the upper limit of detection was 10 mM. Using a silver electrode with 0.01 M NaOH electrolyte, a simple and yet sensitive electrochemical system could enable a real-time field-deployable nitrate sensor that meets the demands of various research communities. The interference study showed that a few ionic species (PO_4^{3-}, Ca^{2+} and Sr^{2+}) in 1000 μM present considerable interferences. Therefore, separation of the interfering ions from the analyte may be required for more precise determination of nitrate. Separation of analytes through a monovalent anion-permeable membrane could decrease interference from cations and multiply-charged anions that interfere with our analysis; a primary study on Donnan dialysis of nitrate in an interfering matrix and simultaneous nitrate determination indicates increases in selectivity.[16]

Acknowledgements

We would like to gratefully acknowledge that our research was funded by the NSF and Center for Embedded Network Sensing at UCLA (NSF CCR-0120778).

References

1 National Research Council, *Ground Water Vulnerability Assessment, Predicting relative contamination potential under conditions of uncertainty*, National Academy Press, Washington, DC, 1993, p. 14.
2 C. S. Bruning-Fann and J. B. Kaneene, *Vet. Hum. Toxicol.*, 1993, **35**, 237–253.
3 G. Ellis, I. Adatia, M. Yazdanpanah and S. K. Makela, *Clin. Biochem.*, 1998, **31**, 195–220.
4 J. Kim, Y. Park and T. C. Harmon, *Ground Water Monit. Remediat.*, 2005, **25**, 78–86.
5 Y. Park, J. Kim and T. C. Harmon, in *Extended Abstract Proceedings of the American Water Resources Association Annual Conference*, ed. S. Steward, American Water Resources Association, Seattle, WA, November 7-10, 2005, (CD-ROM) ISBN 1-882132-69-6, TPS-05-3.
6 M. A. Ferree and R. D. Shannon, *Water Res.*, 2001, **35**, 327–332.
7 S. Kage, K. Kudo and N. Ikeda, *J. Chromatogr., B: Biomed. Appl.*, 2000, **742**, 363–368.
8 J. A. Morales, L. S. de Graterol and J. Mesa, *J. Chromatogr., A*, 2000, **884**, 185–190.
9 V. Jedlickova, Z. Paluch and S. Alusık, *J. Chromatogr., B: Anal. Technol. Biomed. Life Sci.*, 2002, **780**, 193–197.
10 T. Miyado, Y. Tanaka, H. Nagai, S. Takeda, K. Saito, K. Fukushi, Y. Yoshida, S. Wakida and E. Niki, *J. Chromatogr., A*, 2004, **1051**, 185–191.
11 M. J. Moorcroft, J. Davis and R. G. Compton, *Talanta*, 2001, **54**, 785–803.
12 C. M. A. Brett and A. M. O. Brett, *Electrochemistry: Principle, Methods, and Applications*, Oxford University Press, New York, 1993, p. 206.
13 M. Badea, A. Amine, G. Palleschi, D. Moscone, G. Volpe and A. Curulli, *J. Electroanal. Chem.*, 2001, **509**, 66–72.
14 J. R. C. da Rocha, L. Angnes, M. Bertotti, K. Araki and H. E. Toma, *Anal. Chim. Acta*, 2002, **452**, 23–28.
15 C. C. Liu, P. J. Hesketh and G. W. Hunter, *Interface*, 2004, **13**(2), 22–27.
16 D. Kim, I. B. Goldberg and J. W. Judy, *Proc. Electrochem. Soc.*, 2004, **2004–08**, 223–231.
17 Z. Liu, X. Xi, S. Dong and E. Wang, *Anal. Chim. Acta*, 1997, **345**, 147–153.
18 N. G. Carpenter and D. Pletcher, *Anal. Chim. Acta*, 1995, **317**, 287–293.
19 L. H. Larsen, T. Kjaer and N. P. Resvsbech, *Anal. Chem.*, 1997, **69**, 3527–3531.
20 D. Pletcher and Z. Poorabedi, *Electrochim. Acta*, 1979, **24**, 1253–1256.
21 A. G. Fogg, S. P. Scullion and T. E. Edmonds, *Analyst*, 1989, **114**, 579–581.
22 H. Li, D. H. Robertson, J. Q. Chambers and D. T. Hobbs, *J. Electrochem. Soc.*, 1988, **135**, 1154–1158.
23 R. J. Davenport and D. C. Johnson, *Anal. Chem.*, 1973, **45**, 1979–1980.
24 J. D. Genders, D. Hartsough and D. T. Hobbs, *J. Appl. Electrochem.*, 1996, **26**, 1–9.
25 S. Cattarin, *J. Appl. Electrochem.*, 1992, **22**, 1077–1081.
26 M. Fedurco, P. Kedzierzawski and J. Augustynski, *J. Electrochem. Soc.*, 1999, **146**, 2569–2572.
27 J. Krista, M. Kopanica and L. Novotny, *Electroananlysis*, 2000, **12**, 199–204.
28 W. J. Plieth, in *Encyclopedia of Electrochemistry of the Elements*, ed. A. J. Bard, Marcel Dekker, New York, 1978, pp. 321–479.
29 S. N. Davis and R. J. M. DeWiest, *Hydrogeology*, Wiley, New York, 1966, p. 111.
30 E. R. Savinova, E. Walse and K. Doblhofer, *Electrochim. Acta*, 1998, **44**, 1341–1348.
31 E. R. Savinova, P. Kraft, B. Pettinger and K. Doblhofer, *J. Electroanal. Chem.*, 1997, **430**, 47–56.
32 A. G. Fogg, S. P. Scullion, B. J. Birch and T. E. Edmonds, *Analyst*, 1991, **116**, 573–580.
33 J. Davis, M. J. Moorcroft, S. J. Wilkins, M. F. Cardosi and R. G. Compton, *Analyst*, 2000, **125**, 737–742.
34 M. E. Bodini and D. T. Sawyer, *Anal. Chem.*, 1977, **49**, 485–489.
35 G. L. Lundquist, G. Washinger and J. A. Cox, *Anal. Chem.*, 1975, **47**, 319–322.
36 C. Colombo and C. M. G. van den Berg, *Anal. Chim. Acta*, 1998, **377**, 229–240.
37 H. B. Hanekamp, W. H. Voogt, P. Bos and R. W. Frei, *Anal. Chim. Acta*, 1980, **118**, 81–86.
38 J. N. Barisci and G. G. Wallace, *Electroanalysis*, 1992, **4**, 323–326.
39 A. Trojanek and K. Holub, *Anal. Chim. Acta*, 1980, **121**, 23–28.
40 A. J. Bard and L. R. Faulkner, *Electrochemical Methods: Fundamentals and Applications*, Wiley, New York, 2nd edn, 2001, pp. 172–173.
41 D. R. Lide, in *CRC Handbook of Chemistry and Physics*, ed. D. R. Lide, CRC, Boca Raton, FL, 86th edn, 2005, pp. 5–77.
42 K. Aoki and J. Osteryoung, *J. Electroanal. Chem.*, 1984, **160**, 335–339.
43 P. J. Lingane, *Anal. Chem.*, 1964, **36**, 1723–1726.
44 J. B. Flanagan and L. Marcoux, *J. Phys. Chem.*, 1973, **77**, 1051–1055.
45 Z. G. Soos and P. J. Lingane, *J. Phys. Chem.*, 1964, **36**, 3821–3828.
46 D. M. Morgan and S. G. Weber, *Anal. Chem.*, 1984, **56**, 2560–2567.
47 J. T. Long and S. G. Weber, *Anal. Chem.*, 1988, **60**, 2309–2311.
48 A. J. Bard and L. R. Faulkner, *Electrochemical Methods: Fundamentals and Applications*, Wiley, New York, 2nd edn, 2001, p. 163.
49 P. W. J. M. Boumans, in *Inductively Coupled Plasma Emission Spectroscopy, part 1: methodology, instrumentation, and performance*, ed. P. W. J. M. Boumans, Wiley, New York, 1987, pp. 102–107.
50 H. Kaiser, *Anal. Chem.*, 1970, **42**, 26A–59A.